Atlastins mediate selective autophagy of the endoplasmic reticulum

Jin Rui Liang[1,2], Emily Lingeman[1,2], Saba Ahmed[1,2], Jacob Corn[1,2]*

[1]Innovative Genomics Institute, University of California, Berkeley, CA 94720

[2]Department of Molecular and Cell Biology, University of California, Berkeley, CA 94720

*Correspondence: jcorn@berkeley.edu

ABSTRACT

The selective lysosomal degradation (autophagy) of entire organelles is required for cellular homeostasis, and its dysregulation is involved in degenerative disorders such as Parkinson's Disease. While autophagy of mitochondria (mitophagy) is becoming better understood, other forms of organelle autophagy are relatively unexplored. Here we develope multiple quantitative assays to measure organelle autophagy using flow cytometry, microscopy, and Western blotting. Focusing on autophagy of the endoplasmic reticulum (ER-phagy), we show that these assays allow facile measurement of ER-phagy, and that ER-phagy is inhibited by knockdown of either core autophagy components or the recently reported FAM134B ER-phagy receptor. Using these assays, we further identify that Atlastins, the ER-resident GTPases involved in ER membrane morphology, are key positive effectors of ER-phagy. Atlastin-depleted cells have decreased ER-phagy under starvation conditions, and Atlastin's role in ER-phagy requires both a functional GTPase domain and proper ER localization. The three Atlastin family members functionally compensate for one another during ER-phagy and may form heteromeric complexes with one another. We also find that Atlastins act downstream of the FAM134B ER-phagy receptor. We propose that during ER-phagy, Atlastins remodel ER membrane to separate pieces of FAM134B-marked ER for efficient autophagosomal engulfment. Human mutations in Atlastins led to

hereditary spastic paraplegia, and our results suggest that this disease may be linked to deficiencies in ER-phagy rather than ER morphology.

Introduction

The selective autophagy of organelles (organellophagy) constitutes a major part of cellular proteostasis and homeostasis. Dysregulation in organellophagy particularly impacts differentiated cells, such as neurons. The most notable example is mitophagy, whereby loss-of-function mutations of mitophagy proteins such as PARKIN and PINK1 have been linked to neurodegenerative diseases such as Parkinson's Disease[1]. It is now clear that the endoplasmic reticulum (ER) can also be degraded via ER-specific autophagy (ER-phagy).

The endoplasmic reticulum (ER) is a multifunctional organelle that is the major site for protein and lipid synthesis, as well as the quality control of newly synthesized proteins. To prevent the accumulation of toxic protein aggregates, the ER harbors a well-studied quality control pathway known as *ER-A*ssociated *D*egradation (ERAD), in which misfolded ER proteins are extracted for destruction by the proteasome[2]. However, under certain conditions such as starvation, fragments of the ER can also be degraded via ER-phagy[3,4].

During ER-phagy, fragments of the ER are engulfed in their entirety by autophagosomes and sent for destruction in acidified lysosomes. This process is analogous to the lysosome-mediated degradation of mitochondria (mitophagy). Originally described in yeast, ER-phagy has recently been demonstrated to mediate ER degradation in higher eukaryotic cells[3,6,7]. Two ER-membrane surface proteins with conserved LC3-interacting regions (LIRs), FAM134B and RTN3L, can act as specific autophagy receptors for distinct parts of the ER[8,9]. In addition, SEC62, a component of the ER translocon, and CCPG1, a ER stress-induced ER-phagy receptor, have also

47 been shown to play a role in ER degradation[10,11]. These specialized ER-phagy receptors allow
48 portions of the larger ER network to be shunted to the core autophagy pathways. ER-phagy is
49 therefore connected to bulk autophagy of the cytoplasm, but may have dedicated upstream logic,
50 signals, and mediators that are only beginning to be elucidated. For example, unlike cytoplasm, the
51 ER is composed of a highly interconnected network that presumably must be separated prior to
52 autophagosomal engulfment. It is currently unclear how the ER network is packaged into discrete
53 components for delivery to autophagosomes by ER-phagy receptors.

54 Dynamin-like GTPases are dimeric, membrane-tethered proteins that are involved in
55 membrane fusion and fission. Depending on their subcellular localization, these GTPases play
56 important roles in regulating the morphology of the targeted organelles[12,13]. For example,
57 Mitofusins (MFNs) and Optic Atrophy 1 (OPA1) are involved in the dynamic fusion and fission of
58 mitochondria. MFNs and OPA1 can also be post-translationally modified and regulated to signal
59 the remodeling of mitochondria during mitophagy[14,15].

60 Analogous to MFNs and OPA1, Atlastins (ATLs) are a group of three ER-integral membrane
61 proteins that maintain the ER in a reticular network during normal homeostasis. ATLs contain an
62 N-terminal GTPase domain and two transmembrane helices close to the C-terminus that span the
63 ER membrane, such that both N and C-termini face the cytosol (**Supp Fig. 1A**). Atlastins are
64 required for the formation of three-way junctions that build the characteristic inter-connected,
65 web-like network of the ER. Depletion of ATLs leads to the collapse of the ER network into long
66 threads[16-18].

67 Drawing analogy to the roles of MFNs and OPA1 in mitochondrial morphology and
68 mitophagy and reasoning that the ER must be remodeled prior to autophagic engulfment, we
69 hypothesized that ATLs might facilitate ER-phagy. We developed several new assays to measure

70 organelle autophagy, with a focus on ER-phagy. With these assays in hand, we used CRISPR
71 transcriptional inhibition (CRISPRi) to show that ATLs are required for ER-phagy in human cells
72 during nutrient starvation. The three human ATL family members are expressed at different levels
73 in various cell types and are functionally redundant during ER-phagy. In cells that predominantly
74 express ATL2, we find that ER-phagy requires the N-terminal GTPase domain, proper ER
75 localization through the transmembrane domain, and a C-terminal helical tail that is also required
76 for ER membrane remodeling. Overexpression of FAM134B is sufficient to induce ER-phagy and
77 partial loss of ATL2, suggesting that ATL2 could be a remodeling factor for the same ER
78 subdomain marked by FAM134B. However, removal of ATL2 during FAM134B overexpression
79 abrogates ER-phagy. Our results uncover a new mediator of ER-phagy that we propose is required
80 to remodel and separate the ER components marked for destruction by the FAM134B ER-phagy
81 receptor.
82
83 **Results**
84 **Quantitative assays for ER-phagy**
85 One of the obstacles in studying ER-phagy is the paucity of robust markers to monitor the
86 process[3,8,9]. Commonly used ER protein markers such as calnexin (CANX), PDI, CLIMP63, TRAF-α
87 and REEP5 exhibit only a marginal decrease in protein levels during ER-phagy, and it is difficult to
88 use them to establish quantitative measures of ER-phagy. To overcome these limitations, we
89 developed two complementary assays for ER-phagy.
90 Firstly, we developed a quantitative ER-Autophagy Tandem Reporter (EATR) system that
91 fuses a commonly used tandem eGFP-mCherry autophagic reporter to RAMP4, a subunit of the ER
92 translocon complex (**Fig. 1A**)[19]. EATR is designed such that the fluorescent proteins point towards

93 the cytoplasm and relies on the lowered stability of eGFP relative to mCherry when delivered to
94 the acidic environment of the lysosome. Cytosolic ER (pH~7) should be fluorescent in both the
95 eGFP and mCherry channels, whereas ER within a lysosomal vesicle (pH<4) would lose eGFP
96 fluorescence but retain mCherry. This system is inspired by the eGFP-mCherry-LC3 reporter
97 system that is commonly used to study bulk autophagy[20]. This system has also previously been
98 used to show that eGFP-mCherry-FAM134B is degraded via the lysosomal pathway[8]. We placed
99 the reporter under the control of a doxycycline-inducible promoter to induce expression in a
.00 defined time period, and hence follow a bolus of ER as it transitions from cytoplasmic to lysosomal
.01 and is finally degraded (**Fig. 1B**).

.02 We created stable HCT116 cell lines harboring the doxycycline-inducible EATR construct.
.03 Using microscopy, we found that EATR is localized to the ER when cells are grown in complete
.04 media ("fed" condition). Transitioning reporter cells from "fed" to Earl's Buffered Saline Solution
.05 (EBSS, "starved" condition) induces the formation of mCherry-only ER puncta that are recruited
.06 the a perinuclear region, consistent with reports that lysosomes are perinuclear and that
.07 autophagic ER cargoes are trafficked to a perinuclear space (**Fig. 1C**) [8,21]. Treatment with
.08 folimycin, an inhibitor of the lysosomal proton pump, rescued GFP fluorescence in perinuclear ER
.09 (**Fig. 1C**). Co-labeling of the ER and lysosome using mCherry-RAMP4 and GFP-LAMP2,
.10 respectively, further validated that starvation indeed recruits ER to the lysosome, as evident by
.11 the co-localization of mCherry-RAMP4 puncta within GFP-LAMP2 structures (**Supp Fig. 1B**).

.12 We next tested whether EATR could be used to quantify the extent of ER-phagy in a given
.13 cell using flow cytometry. Theoretically, relative change in eGFP and mCherry fluorescence
.14 intensities should report on delivery of the ER to the acidic lysosomal environment (**Fig. 1D**). We
.15 first validated that doxycycline induction results in double expression of mCherry and eGFP, with

each cell having roughly equal amounts of mCherry and eGFP fluorescence. Upon starvation, we observed a decrease in eGFP signal but not mCherry fluorescence, resulting in a shift of cell population into the "acidified ER" gate (**Fig. 1D and E**). Consistent with our microscopy results, folimycin treatment rescued eGFP fluorescence on the ER, presumably due to de-acidification of the lysosome. Quantifying the number of cells that fall into the acidified ER gate yields a metric of ER-phagy that is reproducible between biological replicates (**Fig. 1E**). In sum, we find that the EATR system is capable of measuring ER-phagy both visually by microscopy and quantitatively by flow cytometry.

Encouraged by the results with EATR, we adapted the tandem reporter system to study other organellophagies by fusing the tandem fluorescent reporters to different organelle surface proteins, including TOM20 for mitophagy, PMP34 for pexophagy and LAMP1 for lysophagy (**Fig. 1F**). Similar to the EATR construct, the tandem fluorescent reporters were fused to the organelle-specific protein such that they point towards the cytoplasm and allow for the detection of pH change upon lysosomal localization. In all cases, we observed robust and characteristic localization of all tandem fluorescent reporters to their expected organelles upon doxycycline induction (**Fig. 1G**).

We further wanted an orthogonal assay for ER-phagy that does not depend upon a change in fluorescence and took inspiration from bulk autophagy assays in yeast that measure lysosomal cleavage of GFP from LC3 as a readout for autophagy[22]. GFP-LC3 is effective in yeast but not human cells, due to differences in lysosomal acidification[19], but we reasoned that the apparent stability of mCherry in the flow assay could be a replacement for GFP to measure fluorescent tag separation during autophagy. We found that a stably expressed mCherry-RAMP4 fusion (lacking eGFP) is cleaved to free mCherry during starvation, such that Western blotting for mCherry yields

.39 two distinct bands (**Fig. 1H**). Treatment with folimycin prevents release of mCherry, indicating
.40 that this separation reports on the internalization of ER by lysosomes (**Fig. 1I**). For simplicity, we
.41 refer to this Western blot assay as m<u>C</u>herry-<u>C</u>leavage from <u>ER</u> (CCER). CCER allows for more
.42 sensitive detection of ER-phagy as opposed to measurement of endogenous ER protein
.43 degradation, since the appearance and accumulation of the mCherry band from autophagocytosed
.44 portion of the ER provides a more definitive readout and more obvious fold change than the
.45 marginal loss of endogenous ER proteins relative to the rest of the ER (**Supp Fig. 1C**). Importantly,
.46 the timecourse of ER-phagy measured by CCER is consistent with measurements made using
.47 endogenous ER resident proteins (**Sup Fig. 1D**).

.48 We further validated that both the EATR and CCER assays are bona fide reporters of ER-
.49 phagy by knocking down the FAM134B ER-phagy receptor using short-hairpin RNA[8]. FAM134B
.50 depletion led to significant inhibition of ER-phagy as measured by both EATR and CCER (**Fig. 2A-**
.51 **C**). Conversely, we found that overexpression of wild type FAM134B strongly induced ER-phagy in
.52 both the EATR and CCER systems even in fed conditions, consistent with the previous reports that
.53 FAM134B overexpression is sufficient to trigger ER-phagy (**Fig. 2D and E, Supp Fig. 2A**)[8].
.54 Overexpression of FAM134B with the LIR mutated (FAM134B-LIRmut) did not induce ER-phagy.
.55

.56 **Atlastin knockdown inhibits ER-phagy**

.57 Atlastins (ATLs) are ER-resident GTPases involved in ER remodeling, and so represent
.58 promising candidates to separate ER for delivery to autophagosomes during ER-phagy. Since
.59 Atlastin 1 (ATL1) is preferentially expressed in neuronal cells, we wondered if other Atlastins are
.60 differentially expressed in other cell lines[17,23]. Using Western blotting, we found that the levels of
.61 each Atlastin vary remarkably in different cellular contexts (**Supp Fig. 3A**). Consistent with

.62 previous reports, neuroblastoma SH-SY5Y cells have high level of ATL1 relative to ATL2 and
.63 ATL3[17]. However, in other cell lines, ATL1 can be completely absent. Across the panel of cell lines
.64 tested, we generally found that there are one or two dominantly expressed Atlastins in each cell
.65 line. For example, RPE1 cells only express ATL3 but HepG2 cells only express ATL2. In HCT116
.66 cells, ATL2 is the dominant Atlastin relative to ATL1 and ATL3.

.67 We stably knocked down ATL1, ATL2 and ATL3 via CRISPR-transcriptional inhibition
.68 (CRISPRi) in both EATR HCT116-CRISPRi and CCER HCT116-CRISPRi cells that stably express
.69 catalytically inactive dCas9 fused with a KRAB transcriptional repressor domain (dCas9-KRAB)[24].
.70 As a control, we knocked down ULK1, a central autophagic regulator kinase required for all forms
.71 of autophagy. During starvation, EATR flow cytometry showed that knockdown of ULK1 was
.72 sufficient to inhibit ER-phagy, consistent with ER-phagy proceeding through the canonical
.73 autophagy pathway (**Fig. 3A, Supp Fig. 3B**).

.74 We then used CRISPRi to stably knock down ATL1, ATL2, and ATL3 in hCT116 cells, which
.75 express high levels of ATL2. The knockdown efficiency of the sgRNAs for ATL1 and ATL3 were
.76 variable, but there was no correlation between sgRNA knockdown efficiency and the extent of ER-
.77 phagy (**Supp Fig. 3B- D**). Conversely, we found that depletion of ATL2 inhibited ER-phagy in both
.78 EATR and CCER assays, consistent with a role in ER-phagy (**Fig. 3A, Supp Fig. 3C-E**). Moreover,
.79 the extent of ER-phagy inhibition correlated very well with the knockdown efficiency of each ATL2
.80 guide RNA (**Fig. 3B**). We further validated that ATL2 is required for ER-phagy using an exon-
.81 targeting ATL2 small interfering RNA (siRNA), and found that siATL2 phenocopies sgATL2's
.82 inhibition of ER-autophagy (**Supp Fig. 3F and G**).

.83 Using CCER, we also observed less accumulation of cleaved mCherry in both ULK1 and
.84 ATL2 depleted cells (both sgRNA and siRNA) compared to the non-targeting control cells,

consistent with inhibition of ER-phagy observed with EATR (**Fig. 3C, Supp Fig. 3E and G)**. However, ULK1 knockdown also resulted in the accumulation of more LC3-I and less conversion into LC3-II, indicating the expected block in general autophagy (**Fig 3C, Supp Fig. 3G**). In contrast, ATL2 depletion by either sgRNA or siRNA did not affect the degradation of LC3, suggesting no inhibition of general autophagy (**Fig. 3C, Supp Fig. 3G**).

We further used confocal microscopy to investigate the effect of ATL2 knockdown on ER-phagy using CCER cells. We observed that sgULK1 and sgATL2 cells show less mCherry-RAMP4 puncta that co-localize with the LAMP2 lysosomal marker (**Fig. 3D and E**). Combined with robust autophagy progression in ATL2-depleted cells, this suggests that ATL2 depletion prevents targeted ER from autophagic degradation, a role that is fitting with the ER localization of ATL2 and its known roles in the regulation of ER morphology.

ATL1, ATL2 and ATL3 can functionally compensate for one another during ER-phagy

ATL1, ATL2, and ATL3 have highly similar sequences, with 62-65% overall protein homology and especially at their GTPase domains (**Supp Fig. 4A**). To ask whether the various Atlastins can perform similar functions during ER-phagy, we stably re-expressed cDNAs for ATL1, ATL2 or ATL3 in HCT116 cell lines that are stably knocked down for ATL2. During starvation-induced ER-phagy, re-expression of any one of the three Atlastins was sufficient to rescue ER-phagy (**Fig. 3F and G, Supp Fig. 4B**). By contrast, truncated forms of each Atlastin lacking the ER-localizing transmembrane region (ΔTM) fail to rescue ER-phagy. In addition, immunoprecipitation of ATL2 showed interaction with ATL3 in a manner that is dependent on the GTPase domain but not the TM or C-terminal helix as evident by the lack of interaction with the dimerization defective Arg244Gln (R244Q) mutant but stable interaction with the other constructs (**Supp Fig. 4C**)[17]. This

208 indicates that ATL2 may form a heterodimer with ATL3. Overall, ATL1, ATL2 and ATL3 appear to
209 be functionally interchangeable during ER-phagy and their ER localization is required for this
210 function.
211
212 **ATL2 acts downstream of FAM134B during ER-phagy**
213 Previous studies established FAM134B as an ER surface receptor with LC3 interacting
214 regions (LIRs) that recruits autophagic components to the ER. Since ATLs are also localized on the
215 ER membrane, it is possible that they could also play a similar role in autophagosome recruitment.
216 However, while HA-FAM134B co-immunoprecipitates with LC3 in an LIR-dependent manner,
217 ATL2 does not bind to LC3, suggesting that ATL2 serves a different role during ER-phagy (**Supp**
218 **Fig. 5A**).
219 Since FAM134B and ATL2 appear to serve distinct functions during ER-phagy, we asked if
220 they act in the same pathway. To this end, we transiently knocked down ATL2 in FAM134B
221 overexpressing cells that upregulate ER-phagy even in the fed state. FAM134B overexpression
222 enhances the degradation of ATL2 under fed condition, and ATL2 protein level is further reduced
223 upon starvation, suggesting that FAM134B is upstream of ATL2 (**Fig. 4A**). We also found that
224 ATL2 is epistatic to FAM134B overexpression, such that the knockdown of ATL2 reduces
225 FAM134B-induced ER-phagy in both fed and starved conditions (**Fig. 4A and B, Supp Fig. 5B**).
226 Hence, it appears that ATL2 is downstream of FAM134B during ER-phagy.
227
228 **Atlastin dimerization and GTPase activity are required for ER-phagy**
229 Using ATL2 as an archetypal Atlastin in HCT116 cells, we next asked what molecular
230 features of Atlastins are required for ER-autophagy versus ER morphology. During the

231 maintenance of ER morphology, the various domains of ATL2 perform sequential functions in a
232 GTP-dependent fashion (**Fig. 5A**)[18]. Upon GTP loading at the GTPase domain, ATL2 is primed for
233 dimerization with another activated ATL2, leading to ER membrane tethering. This is closely
234 followed by ER membrane fusion, a process that requires the C-terminal helix for locaized
235 membrane destabilization{Moss:2011eo}. We generated several constructs of ATL2 to interrogate
236 and compare the importance of each domain for ER morphology and ER-phagy (**Fig. 5A**).

237 Overexpressed wild-type ATL2 localizes to the ER network, forming a distinctive reticular
238 network with interspersed puncta at the three-way junctions of the ER (**Fig. 5B**). During
239 starvation, stable re-expression of wild-type ATL2 restored the diminished ER-phagy caused by
240 depletion of ATL2 (**Fig. 5C and D, Supp Fig. 6A**).

241 In the presence of endogenous ATL2, overexpressed ATL2 lacking the transmembrane
242 helices (ATL-ΔTM) did not localize to a clearly ER structure. Instead, this construct caused
243 mCherry-RAMP4 marked ER to collapse into an aggregated perinuclear cluster with radiating
244 strands (**Fig. 5B**). This dominant negative ER morphology phenotype is consistent with previous
245 reports that free ATL2 GTPase domains serve as potent, dosage-dependent inhibitors to
246 endogenous ATL2 by preventing dimerization between endogenous ATL2 molecules and
247 inhibiting ER membrane fusion[18]. We found that re-expression of ATL2-ΔTM during ATL2
248 knockdown was unable to rescue ER-phagy (**Fig. 5C and D, Supp Fig. 6A**).

249 We then interrogated the requirement of membrane fusion for ER morphology
250 maintenance and ER-phagy using a truncated form of ATL2 that retains the transmembrane
251 regions but lacks the C-terminal helical domain (ATL2-ΔCterm), We found that overexpression of
252 ATL2-ΔCterm was not dominant negative and had a similar ER morphology to that of wild-type
253 ATL2 at basal state (**Fig. 5B**). ATL2-ΔCterm expression during ATL2 knockdown partially rescues

254 ER-phagy, indicating that the membrane fusion function of ATL2 is required during ER-phagy (**Fig.**
255 **5C and D, Supp Fig. 6A**).

256 We finally overexpressed an ATL2 mutant that renders the protein incapable of dimerizing
257 (Arg244Gln)[17]. Arg244Gln (R244Q) is equivalent to the human pathogenic Arg217Gln mutation in
258 ATL1 that is implicated in hereditary spastic paraplegia (HSP). Overexpression of Arg244Gln led
259 to ER elongation and lack of reticular connections, but without the collapsed structures observed
260 with the ΔTM construct (**Fig. 5B**). The ATL2-R244Q mutant was also unable to rescue the loss of
261 ER-phagy induced by ATL2 knockdown. Overall, our data shows that the functional GTPase
262 domain and proper ER localization of ATL2 are required for both ER morphology and ER-phagy
263 regulations (**Fig. 5C and D, Supp Fig. 5A**). Together with our data which indicate that ATL2 is
264 downstream of FAM134B, we propose that FAM134B is the ER-phagy receptor that recruits LC3 to
265 the ER, and Atlastins are responsible for membrane remodeling to deliver FAM134B-marked ER to
266 the autophagy (**Fig. 5E**).

267

268 **Discussion**

269 The mechanisms underlying autophagy of the endoplasmic reticulum are just beginning to
270 be elucidated. We developed two independent systems, EATR and CCER, to report on specific
271 degradation of the ER. The flow cytometry, fluorescence microscopy, and Western blotting assays
272 derived from these systems offer sensitive and quantitative readouts for the progression of ER-
273 phagy. Considering that only a small fraction of ER is actually targeted for ER-phagy at one time,
274 EATR and CCER are more sensitive than measuring endogenous ER protein degradation[3,25]. While
275 EATR provides a quantitative measurement at an individual cell level, CCER can be combined with
276 simultaneous immunoblotting of other ER and autophagy proteins to provide more mechanistic

277 insight into ER-phagy. EATR and CCER therefore serve as complimentary systems to orthogonally
278 explore ER-phagy.

279 Using EATR and CCER, we found that the ER-resident membrane organizing Atlastin
280 GTPases are required for ER-phagy. While ER-resident autophagy receptors such as FAM134B
281 have been identified, the machinery responsible for isolating ER fragments for delivery to
282 autophagosomes remains unclear[25]. During mitophagy, mitochondria-resident GTPases such as
283 MFNs and MIROs assume a passive role during mitophagy, in the sense that they are ubiquitylated
284 for proteasomal degradation and subsequently lead to mitochondria fragmentation prior to
285 autophagosomal engulfment[15,26]. In contrast, our data suggest that Atlastins play an active role
286 during ER-phagy**.** Loss of Atlastins represses ER-phagy, and functional Atlastin domains required
287 for ER morphology are also required for ER-phagy. We also found that ATL2 depletion impedes
288 ER-phagy induced by FAM134B overexpression, indicating that ATL2 acts downstream of
289 FAM134B during ER-phagy. Since FAM134B-induced ER-autophagy leads to reductions in ATL2
290 levels, it also appears that Atlastins act both as an effector and a cargo of FAM134B-mediated ER-
291 phagy.

292 Our functional studies of ATL2 indicate that a functional GTPase domain, ER localization,
293 and C-terminal helix are all required during ER-phagy. While we cannot conclusively rule out
294 additional roles of Atlastin during starvation, our data suggest that Atlastin's role during ER-phagy
295 is closely related to its role of ER membrane remodeling. We propose that FAM134B recruits
296 autophagosomes to ER destined for autophagic degradation, and Atlastins locally remodel the
297 FAM134B-marked ER for packaging into autophagosomes (**Fig. 5E**). ATL1 in particular has known
298 roles in in ER vesiculation during normal homeostasis, and this function may be co-opted during
299 ER-phagy[23].

300 Dysregulation in organelle quality control and turnover has detrimental effects on cell
301 fitness and has been linked to multiple diseases. Mounting evidence points towards the
302 importance of organelle quality control for non-regenerative cell types such as neurons. For
303 example, mutations in mitophagy regulators such as PINK1 and Parkin have been reported in
304 patients of Familial Parkinsonism[27]. The FAM134B ER-phagy receptor has likewise been
305 implicated in hereditary sensory neuropathy, a genetic disorder that results in degeneration of
306 sensory nerves of the extremities[28]. Notably, an ATL1 loss-of-function mutation (SPG3A) has been
307 associated with hereditary spastic paraplegia (HSP)[29]. HSP is characterized by the loss of axonal
308 cortical motor neurons, resulting in progressive weakness and spasticity of the lower limbs. ATL1
309 mutations have previously been proposed to lead to HSP through dysregulation of ER
310 morphology[30]. Considering the similarities in clinical manifestation between FAM134B and ATL1
311 mutations, combined with our data demonstrating that ATLs act downstream of FAM134B during
312 ER-phagy, we suggest that an inability to execute ER-phagy might be a contributing factor to HSP
313 caused by ATL1 mutations. It remains to be seen whether HSP is concretely caused by deficits in
314 ER-phagy or dysfunctional ER morphology, and further mechanistic studies will hopefully shed
315 light on the molecular basis of the disease.
316
317 **Figure 1: Development of sensitive and quantitative assays to measure ER-phagy**
318 (A) Schematic illustration of the Doxycycline-inducible ER-Autophagy Tandem Reporter (EATR)
319 assay featuring a tandem mCherry-eGFP tagged to RAMP4. The environmental pH of cytosolic
320 ER is pH~7, allowing both eGFP and mCherry to fluoresce normally. During ER-phagy, ER is
321 engulfed and degraded within the lysosome (pH<4), causing the protonation of eGFP and
322 quenching of its fluorescence whereas mCherry protein is relatively stable in the acidic

323 environment. Thus, a switch from $GFP^+/mCherry^+$ to $GFP^-/mCherry^+$ indicates the occurrence
324 of ER-phagy.
325 (B) Schematic of the application of EATR to measure ER-phagy by fluorescence-activated cell
326 sorting (FACS). The progression of ER-phagy is sequentially labeled from 1 to 3. (1) Upon Dox-
327 induction at basal 'fed' state, cells express both eGFP and mCherry fluorescence (yellow
328 triangle). (2) During starvation, a fraction of the ER undergoes ER-phagy and loses eGFP
329 fluorescence due to localization within lysosome, resulting in a population shift to the left (red
330 triangle). (3) Complete ER-phagy (with all ER containing the reporter being degraded) will
331 result in complete loss of both eGFP and mCherry expression. Note that complete
332 relocalization of cell population to the bottom left box (complete ER degradation) has yet to be
333 observed as only a small fraction of ER are being degraded during starvation.
334 (C) HCT116 cells expressing the EATR construct show that the reporter localizes to the ER (See
335 also **Supp Fig. 1B**). Starvation induces the formation of perinuclear mCherry-only puncta that
336 colocalizes with the lysosome (Supp Fig. 1B). Neutralization of the lysosome using folimycin
337 rescues eGFP fluorescence. Insets represent 6-fold enlargement of the boxed area. Scale bar
338 represents 20μm.
339 (D) HCT116 cells expressing the EATR reporter were doxycycline-induced (4μg/ml) and then
340 starved for 16hrs in EBSS with or without folimycin (100nM). mCherry and eGFP fluorescence
341 was then measured by flow cytometry. The 'acidified ER' gate was drawn to exclude the cell
342 population at 'fed' condition. Any cell that moves out of the gate represents a decrease in eGFP
343 fluorescence and hence has more 'acidified ER', indicative of cells undergoing ER-phagy.
344 Treatment with folimycin to abrogate lysosomal acidification moves all cells out of the
345 'acidified ER' gate.

346 (E) Flow cytometry measurement of ERphagy based on (C) is plotted as percentage of cells with
347 more 'acidified ER'. Data presented as mean±SD of three biological replicates. P-value indicates
348 two-tailed unpaired T-test with ***P < 0.0005.
349 (F) Schematic illustration of the organellophagy reporters. All reporters with the exception of
350 EATR are fluorescently tagged at the C-terminus to ensure that the fluorescent tag faces the
351 cytosol.
352 (G) U2OS cells expressing each tandem fluorescent reporters with doxycycline regulation. Images
353 were taken at fed state. Scale bar represents 20μm.
354 (H) Schematic illustration of mCherry-Cleaved from ER (CCER) assay. ER targeted for degradation
355 results in the lysosomal cleavage of the mCherry tag from RAMP4, resulting in the formation of
356 a smaller, mCherry-only product that can be resolved by Western blotting.
357 (I) HCT116 cells stably expressing CCER were starved for 16hrs in EBSS with or without folimycin
358 (100nM) to measure the accumulation of cleaved mCherry by Western blotting.
359
360 **Figure 2. EATR and CCER detects changes in ER-phagy induced by manipulation of a known**
361 **ER-phagy receptor**
362 (A) EATR HCT116 cells were transfected with short-hairpin RNA targeting FAM134B. Cells were
363 starved for 16hr prior to FACS measurement. Data presented as mean±SD of three biological
364 replicates. P-value indicates one-way ANOVA with Tukey's multiple comparisons test.
365 (B) CCER HCT116 cells were treated as in (A), harvested and Western blotted for the indicated
366 proteins.
367 (C) Densitometry measurement of cleaved mCherry versus full-length mCherry-RAMP4
368 normalized to non-targeting guide RNA (sgNT) at starved condition. Data presented as

369 mean±SD of three biological replicates. P-value indicates one-way ANOVA with Tukey's
370 multiple comparisons test.
371 (D) EATR HCT116 cells stably expressing FAM134B cDNAs (WT or LIRmut) were starved for
372 16hrs prior to FACS measurement. Data presented as mean±SD of three biological replicates.
373 P-value indicates one-way ANOVA with Tukey's multiple comparisons test.
374 (E) CCER HCT116 cells were treated as in (D), harvested and Western blotted for the indicated
375 proteins. A representative blot is shown with quantification from three biological replicates
376 shown in **Supp Fig. 2A**.
377
378 **Figure 3 Atlastin knockdown inhibits ER-phagy**
379 (A) EATR CRISPRi HCT116 cells stably expressing sgRNAs targeting either ULK1 or ATL2 were
380 starved for 16hrs and ER-phagy was quantified by flow cytometry. Data presented as
381 mean±SD of three biological replicates. P-value indicates one-way ANOVA with Tukey's
382 multiple comparisons test.
383 (B) The extent of knockdown from five ATL2-targeting sgRNAs correlates with the extent of ER-
384 phagy inhibition.
385 (C) CCER CRISPRi HCT116 cells stably expressing the sgRNAs shown in (A) were starved for
386 16hrs, harvested and Western blotted for the indicated proteins. A representative blot is
387 shown with the quantification of three biological replicates shown in **Supp Fig. 3E.**
388 (D) CCER CRISPRi HCT116 cells stably-transduced with the indicated sgRNAs were starved for
389 16hrs. Cells were fixed and stained with LAMP2 antibody to visualize the lysosomes. Inset
390 represents 3x enlargement of boxed area. Scale bar represents 20μm.

391 (E) Mean cell quantitation (±SD) of three biological replicates from microscopy study shown in
392 (D). An average of 100 cells per condition was quantified. P-value indicates two-tailed
393 unpaired T-test with **P < 0.005 and *P<0.05.
394 (F) EATR CRISPRi HCT116 cells expressing sgATL2 were stably transduced with the indicated
395 GFP-tagged ATL1, 2 or 3 (WT versus ΔTM) and starved for 16hrs. Data presented as mean±SD
396 of three biological replicates. P-value indicates one-way ANOVA with Tukey's multiple
397 comparisons test.
398 (G) CCER CRISPRi HCT116 cells expressing sgATL2 were stably transduced with the indicated
399 GFP-tagged ATL1, 2 or 3. Cells were starved for 16hrs, harvested and Western blotted for the
400 indicated proteins. A representative blot is shown here with quantification from three
401 biological replicates shown in **Supp Fig. 4B.**
402
403 **Figure 4 Atlastins act downstream of FAM134B-mediated ER-phagy**
404 (A) CCER CRISPRi HCT116 cells stably expressing GFP-FAM134B and sgATL2 were starved for
405 16hrs. Representative Western blot is shown here with the fraction of mCherry cleavage
406 measurement from three biological replicates quantified in **Supp Fig. 5B.**
407 (B) EATR CRISPRi HCT116 cells stably expressing GFP-FAM134B and sgATL2 were starved for
408 16hrs and measured by flow cytometry. Data presented as mean±SD of three biological
409 replicates. P-value indicates one-way ANOVA with Tukey's multiple comparisons test.
410
411 **Figure 5 ER-phagy requires a functional Atlastin GTPase domain and proper ER localization**
412 (A) Schematic of the topology and dimerization of Atlastins to facilitate ER membrane fusion. The
413 different truncations and mutations of ATL2 tested shown underneath.

(B) U2-OS cells expressing mCherry-RAMP4 were transiently transfected with the indicated HA-tagged mutant versions of ATL2 for 24hrs. Cells were then fixed and imaged to visualize the change in ER morphology. Inset represents 3x enlargement of the boxed areas. Scale bar represents 20μm.

(C) EATR CRISPRi HCT116 cells stably expressing sgATL2 and cDNA of ATL2 mutant variants were starved for 16hrs and ER-phagy measured by flow cytometry. Data presented as mean±SD of three biological replicates. P-value indicates one-way ANOVA with Tukey's multiple comparisons test.

(D) CCER CRISPRi HCT116 cells with sgATL2 and stably expressing GFP-tagged version of ATL2 mutants were Western blotted for the indicated proteins. A representative blot is shown here and quantification of three biological replicates shown in **Supp Fig. 6A.**

(E) Our data suggests that Atlastins act downstream of FAM134B and we propose that FAM134B acts as the ER-phagy receptor that recruits LC3 to the ER while Atlastins are involved in ER membrane remodeling to deliver FAM134B-marked ER to the autophagosomes.

Supplementary Figure 1

(A) Schematic illustrating the topology and dimerization of Atlastins during ER membrane fusion. Both the N-terminal GTPase domain and the C-terminal helix faces the cytosol, with two transmembrane helixes spanning the ER membrane. Atlastins dimerize and undergo GTP hydrolysis to facilitate the fusion of two neighbouring ER membranes.

(B) HCT116 cells stably expressing mCherry-RAMP4 and LAMP2-eGFP were starved for 16hrs with or without folimycin treatment. Cells were fixed and imaged to visualize ER and lysosome co-localization. Inset represents 5x enlargement of boxed area. Scale bar represents 20μm.

437 (C) CCER HCT116 cells were starved for the indicated duration in EBSS (+/- folimycin) to measure
438 the loss of ER resident proteins and proteins involved in general autophagy by Western
439 blotting.
440 (D) Densitometry measurement of Western blots in (C). Band intensities were normalized to the
441 highest signal.
442
443 **Supplementary Figure 2**
444 (A) Densitometry measurement from **Fig. 2E** of the ratio of cleaved mCherry band versus full-
445 length mCherry-RAMP4 normalized to the starved GFP-FAM134B-WT sample. Data presented
446 as mean±SD of three biological replicates. P-value indicates one-way ANOVA with Tukey's
447 multiple comparisons test.
448
449 **Supplementary Figure 3**
450 (A) Cell lysates from different cell lines at 'fed' condition were loaded at equal amount to measure
451 the protein expression profiles of ATL1, ATL2 and ATL3.
452 (B) CRISPRi HCT116 cells were stably transduced with sgRNAs targeting ATL1, 2 or 3. Knockdown
453 efficiencies were assessed by qRT-PCR and normalized to β-actin and non-targeting sgRNA
454 (sgNT). Two previously validated ULK1 sgRNAs were used as positive controls.
455 (C) sgRNAs with the best knockdown efficiencies based on qRT-PCR from (B) were transduced
456 into EATR CRISPRi HCT116 cells. Data presented as mean±SD of six biological replicates. P-
457 value indicates one-way ANOVA with Tukey's multiple comparisons test.

458 (D) CCER CRISPRi HCT116 cells were stably transduced with sgRNA targeting the indicated genes
459 and starved for 16hrs. Cell lysates were harvested and Western blotted for the indicated
460 proteins.
461 (E) Densitometry measurement from **Fig 3C** of the ratio of cleaved mCherry band versus full-
462 length mCherry-RAMP4 normalized to the starved NT sample. Data presented as mean±SD of
463 three biological replicates. P-value indicates one-way ANOVA with Tukey's multiple
464 comparisons test.
465 (F) EATR CRISPRi HCT116 cells were transiently transfected with siRNA targeting either ULK1 or
466 ATL2 for 48hrs prior to starvation for 16hrs. Data presented as mean±SD of three biological
467 replicates. P-value indicates one-way ANOVA with Tukey's multiple comparisons test.
468 (G) CCER CRISPRi HCT116 cells were transiently transfected with siRNA targeting either ULK1 or
469 ATL2 for 48hrs prior to starvation for 16hrs. A representative blot is shown.
470
471 **Supplementary Figure 4**
472 (A) Protein sequence alignment between human ATL1, ATL2 and ATL3 performed using Clustal
473 Omega. The boxed areas indicate the respective GTPase and transmembrane domains.
474 (B) Densitometry measurement from **Fig. 3G** of the ratio of cleaved mCherry band versus full-
475 length mCherry-RAMP4 normalized to the starved NT sample. Data presented as mean±SD of
476 three biological replicates. P-value indicates one-way ANOVA with Tukey's multiple
477 comparisons test.
478 (C) HCT116 cells stably expressing HA-tagged ATL2 or its mutant variants were
479 immunoprecipitated with anti-HA antibody to measure interaction with ATL3.
480

481 **Supplementary Figure 5**

482 (A) HEK293T cells were transfected with the indicated HA-tagged constructs for 24hrs. Cells were
483 then treated with folimycin for 2hrs prior to HA-immunoprecipitation and Western blotted for
484 the indicated proteins. The LC3 blot was imaged at two different intensities to visualize the
485 input and the HA-IP lanes.

486 **(B)** Densitometry measurement from **Fig. 4A** of the ratio of cleaved mCherry band versus full-
487 length mCherry-RAMP4 normalized to the starved siNT with FAM134B overexpression
488 sample. Data presented as mean±SD of three biological replicates. P-value indicates one-way
489 ANOVA with Tukey's multiple comparisons test.

490

491 **Supplementary Figure 6**

492 (A) Densitometry measurement from **Fig. 5D** of the ratio of cleaved mCherry band versus full-
493 length mCherry-RAMP4 normalized to the starved NT sample. Data presented as mean±SD of
494 three biological replicates. P-value indicates one-way ANOVA with Tukey's multiple
495 comparisons test.

496

497 1. Pickrell, A. M. & Youle, R. J. The roles of PINK1, parkin, and mitochondrial fidelity in
498 Parkinson's disease. *Neuron* **85,** 257–273 (2015).
499 2. Brodsky, J. L. Cleaning up: ER-associated degradation to the rescue. *Cell* **151,** 1163–1167
500 (2012).
501 3. Mochida, K. *et al.* Receptor-mediated selective autophagy degrades the endoplasmic
502 reticulum and the nucleus. *Nature* **522,** 359–362 (2015).
503 4. Dikic, I. Proteasomal and Autophagic Degradation Systems. *Annu. Rev. Biochem.* **86,** 193–224
504 (2017).
505 5. Deas, E., Wood, N. W. & Plun-Favreau, H. Mitophagy and Parkinson's disease: the PINK1-
506 parkin link. *Biochim Biophys Acta* **1813,** 623–633 (2011).
507 6. Nakatogawa, H. Eating the ER and the nucleus for survival under starvation conditions.
508 *Molecular & Cellular Oncology* 00–00 (2015). doi:10.1080/23723556.2015.1073416
509 7. Schuck, S., Gallagher, C. M. & Walter, P. ER-phagy mediates selective degradation of
510 endoplasmic reticulum independently of the core autophagy machinery. *J Cell Sci* **127,**

511 4078–4088 (2014).
512 8. Khaminets, A. *et al.* Regulation of endoplasmic reticulum turnover by selective autophagy.
513 *Nature* **522,** 354–358 (2015).
514 9. Grumati, P. *et al.* Full length RTN3 regulates turnover of tubular endoplasmic reticulum via
515 selective autophagy. *eLife* **6,** 911 (2017).
516 10. Fumagalli, F. *et al.* Translocon component Sec62 acts in endoplasmic reticulum turnover
517 during stress recovery. *Nat Cell Biol* **18,** 1173–1184 (2016).
518 11. Smith, M. D. *et al.* CCPG1 Is a Non-canonical Autophagy Cargo Receptor Essential for ER-
519 Phagy and Pancreatic ER Proteostasis. *Dev Cell* (2017). doi:10.1016/j.devcel.2017.11.024
520 12. McNew, J. A., Sondermann, H., Lee, T., Stern, M. & Brandizzi, F. GTP-dependent membrane
521 fusion. *Annu Rev Cell Dev Biol* **29,** 529–550 (2013).
522 13. Praefcke, G. J. K. & McMahon, H. T. The dynamin superfamily: universal membrane
523 tubulation and fission molecules? *Nature Reviews Molecular Cell Biology* **5,** 133–147 (2004).
524 14. MacVicar, T. D. & Lane, J. D. Impaired OMA1-dependent cleavage of OPA1 and reduced DRP1
525 fission activity combine to prevent mitophagy in cells that are dependent on oxidative
526 phosphorylation. *J Cell Sci* **127,** 2313–2325 (2014).
527 15. Gegg, M. E. *et al.* Mitofusin 1 and mitofusin 2 are ubiquitinated in a PINK1/parkin-
528 dependent manner upon induction of mitophagy. *Human Molecular Genetics* **19,** 4861–4870
529 (2010).
530 16. Ulengin, I., Park, J. J. & Lee, T. H. ER network formation and membrane fusion by
531 atlastin1/SPG3A disease variants. *Mol Biol Cell* **26,** 1616–1628 (2015).
532 17. Rismanchi, N., Soderblom, C. & Stadler, J. Atlastin GTPases are required for Golgi apparatus
533 and ER morphogenesis. *Human molecular …* (2008).
534 18. Moss, T. J., Andreazza, C., Verma, A., Daga, A. & McNew, J. A. Membrane fusion by the GTPase
535 atlastin requires a conserved C-terminal cytoplasmic tail and dimerization through the
536 middle domain. *Proc Natl Acad Sci U S A* **108,** 11133–11138 (2011).
537 19. Mizushima, N., Yoshimori, T. & Levine, B. Methods in Mammalian Autophagy Research. *Cell*
538 **140,** 313–326 (2010).
539 20. Kimura, S., Noda, T. & Yoshimori, T. Dissection of the Autophagosome Maturation Process by
540 a Novel Reporter Protein, Tandem Fluorescent-Tagged LC3. *Autophagy* **3,** 452–460 (2007).
541 21. Korolchuk, V. I. *et al.* Lysosomal positioning coordinates cellular nutrient responses. *Nat Cell*
542 *Biol* **13,** 453–460 (2011).
543 22. Hosokawa, N., Hara, Y. & Mizushima, N. Generation of cell lines with tetracycline-regulated
544 autophagy and a role for autophagy in controlling cell size. *FEBS Lett* **581,** 2623–2629
545 (2007).
546 23. Muriel, M.-P. *et al.* Atlastin-1, the dynamin-like GTPase responsible for spastic paraplegia
547 SPG3A, remodels lipid membranes and may form tubules and vesicles in the endoplasmic
548 reticulum. *J Neurochem* **110,** 1607–1616 (2009).
549 24. Gilbert, L. A. *et al.* Genome-Scale CRISPR-Mediated Control of Gene Repression and
550 Activation. *Cell* **159,** 647–661 (2014).
551 25. Khaminets, A. *et al.* Regulation of endoplasmic reticulum turnover by selective autophagy.
552 *Nature* **522,** 354–358 (2015).
553 26. Liu, S. *et al.* Parkinson's disease-associated kinase PINK1 regulates Miro protein level and
554 axonal transport of mitochondria. *PLoS Genet* **8,** e1002537 (2012).
555 27. Gegg, M. E. & Schapira, A. H. PINK1-parkin-dependent mitophagy involves ubiquitination of
556 mitofusins 1 and 2: Implications for Parkinson disease pathogenesis. *Autophagy* **7,** 243–245

(2011).
28. Ilgaz Aydinlar, E., Rolfs, A., Serteser, M. & Parman, Y. Mutation in FAM134B causing hereditary sensory neuropathy with spasticity in a Turkish family. *Muscle & Nerve* **49,** 774–775 (2014).
29. Namekawa, M. *et al.* Mutations in the SPG3A gene encoding the GTPase atlastin interfere with vesicle trafficking in the ER/Golgi interface and Golgi morphogenesis. *Molecular and Cellular Neuroscience* **35,** 1–13 (2007).
30. Zhu, P.-P., Soderblom, C., Tao-Cheng, J.-H., Stadler, J. & Blackstone, C. SPG3A protein atlastin-1 is enriched in growth cones and promotes axon elongation during neuronal development. *Human Molecular Genetics* **15,** 1343–1353 (2006).

Materials and Method

sgRNA, shRNA, siRNA and cDNA plasmid cloning procedures

Information for the sgRNA sequences targeting the transcription start site (TSS) of each gene were obtained from the Weissman CRISPRi-v2 library[1]**.** In each case, the top 5 guides were cloned into pGL1-library vector (Addgene # 84832) as previously described[1]. Knockdown efficiency for each guide was either validated by qRT-PCR or western blotting. A complete list of all sgRNA constructs used in this study is listed in **Supp Table 1.**

Short hairpin (sh) non-targeting (NT) and shFAM134B were cloned into pLKO.1 puro construct (Addgene #8453) according to protocol available at Addgene website (http://www.addgene.org/tools/protocols/plko/). shRNA sequences used in this study are listed in **Supp Table 1**.

The cDNA of ATL1 was obtained from Harvard PlasmID database (HsCD00326984). cDNAs of ATL2, ATL3 and FAM134B were obtained by PCR amplification of cDNA generated from HCT116 cells. All overexpression constructs were cloned into pLenti-X1-DEST vector (with either neomycin, blastocystin or hygromycin-resistant cassette) via Gibson Assembly[2]. Firstly, a previously cloned pLenti-X1-pEF-mCherry-eGFP-LC3 construct (by LR clonase reaction) was first cut using BamHI and XbaI to liberate the insert. The gene of interest was then Gibson assembled using Gibson Assembly Master Mix (NEB; E2611) together with the desired epitope or fluorescence tag into the pLenti-X1-DEST vector backbone according to manufacturer's instruction. A complete list of all constructs used in this study is listed in **Supp Table 2.**

24

25 *Cell culture*

26 Cell culture was performed at 37°C in a humidified atmosphere containing 5% CO_2.
27 HCT116, HEK293T, MCF7, U2-OS, MDA-MB-468, SH-SY5Y, and U2-OS cells were
28 obtained from the Berkeley Cell Culture Facility. All cell lines were cultured in
29 Dulbecco's Modified Eagle's medium (DMEM) with high glucose. hTERT-RPE1 cells
30 were cultured in DMEM/F12 with high glucose. All culture media were
31 supplemented with 10% fetal bovine serum (FBS), 100 U/ml penicillin (Gibco), 100
32 g/ml streptomycin (Gibco), 0.1mM non-essential amino acids and 1 mM sodium
33 pyruvate (Gibco).

34

35 *Lentiviral packaging and transduction*

36 Lentiviral packaging of all constructs was performed in HEK293T cells using
37 TransIT®-LT1 Transfection Reagent (Mirus) according to manufacturer's
38 instructions. Briefly, plasmids were transfected at a ratio of 1:3 (1μg plasmid to 3μl
39 of TransIT-LT1 reagent). The plasmid composition follows 50% plasmid with target
40 of interest 40% ΔVPR plasmid and 10% VSVG plasmid. Lentiviruses were harvested
41 either at 48hr or 72hr post transfection for transduction. Puromycin treatment was
42 performed at 30μg/ml and Neomycin (G418) treatment was performed at 2mg/ml
43 in HCT116 cells. All antibiotic selections were carried out for at least two passages
44 to ensure complete selection.

45

46 *Transient Transfection of siRNA and plasmids*

47 Transient transfection of plasmids into HEK293T cells for the purpose of
48 immunoprecipitation was performed using TransIT-LT1 whereas transient
49 transfection of plasmids into U2-OS cells were performed using Lipofectamine 3000
50 (Invitrogen) according to manufacturer's instructions at a ratio of 1:3 (1μg plasmid
51 to 3μl of Lipofectamine 3000).

52 Custom ordered siRNA oligoes (Dharmacon) were transiently transfected
53 into targeted cells using RNAiMAX (Invitrogen) according to manufacturer's
54 instructions. For each well of a 12-well plate, 120pmol of siRNA were diluted in 50μl
55 of OptiMEM. 3.6μl of RNAiMAX was diluted in 50μl of OptiMEM. The diluted siRNA
56 was then added to the diluted RNAiMAX mixture and incubated at room
57 temperature for 5min prior to adding into cell culture. A complete list of all siRNA
58 constructs used in this study is listed in **Supp Table 3.**

59

60 G*eneration of CRISPRi HCT116 cells*

61 HCT116 cells were transduced with lentivirus with an EF1a-dCas9-HA-BFP-KRAB-
62 NLS construct to generate a pool of CRISPRi HCT116 cells. Cells were FACS sorted
63 and single-cell seeded based on BFP expression. Individual clones were validated by
64 probing for HA tag expression via Western blot. The clones were transduced with a
65 panel of previously validated sgRNAs (SEL1, SYVN, UBE4A, DPH1 and FUT4) using
66 and knockdown efficiency of each clone was assessed by q-RT-PCR. The selected
67 CRISPRi HCT116 clone was further transfected with either TET-On-mCherry-GFP-
68 RAMP4 (for EATR assay) or mCherry-RAMP4 (for CCER assay) and clonal cell lines
69 were generated for uniform doxycycline response and expression of the ER

70 markers. For simplicity, the two cell lines were named EATR CRISPRi HCT116 and
71 CCER CRISPRi HCT116 cells, respectively.
72
73 *Cell treatments*
74 For both EATR and CCER assays, cells were seeded and grown for 48hrs prior to
75 starvation. In the case of EATR assay, doxycycline was added at 4μg/ml 24hrs prior
76 to starvation to induce the expression of eGFP-mCherry-RAMP4. Cells were 'starved'
77 using Earl's Buffered Saline Solution (EBSS) with calcium, magnesium and phenol
78 red (Invitrogen, Cat. #24010043) to induce ER-phagy. As opposed to 'starved'
79 condition, 'fed' condition indicates incubation in normal DMEM with the usual
80 supplements. Unless stated otherwise, co-treatment with folimycin (Milipore) were
81 performed at 100nM final concentration. All starvation and/or drug treatments
82 were carried out for 16hrs unless otherwise indicated.
83
84 *Quantitative real-time RT-PCR (qRT-PCR)*
85 Cultured cells were harvested for RNA extraction using Direct-zol RNA miniprep kit
86 (Zymogen) according to manufacturer's instructions. One microgram of total RNA
87 was used for reverse transcription using Superscript III First Strand Synthesis
88 SuperMix for qRT-PCR (Invitrogen) according to manufacturer's instructions. qRT-
89 PCR was performed in triplicates using Fast SYBR Green Master Mix (Applied
90 Bioystems) and StepOne Plus Real-Time PCR System (Applied Biosystems). Samples
91 were analyzed with 2-step amplification and melt curves were analysed after 40
92 cycles. The Ct value for test genes was normalized to β-Actin and the expression of

93 each gene was represented as 2-[ΔΔCt] relative to the non-targeting control. All
94 primers used are listed in **Supp Table 4.**
95
96 *Western blotting*
97 After treatment, cells were lysed using RIPA buffer (Milipore) supplemented with
98 Halt Protease inhibitor cocktail (ThermoFisher) and Halt Phosphatase inhibitor
99 cocktail (ThermoFisher). Protein concentration was determined by Bradford Assay
100 (VWR) and NuPAGE LDS Sample Buffer (Invitrogen) was added to the concentration
101 normalized protein samples. Samples were resolved on NU-PAGE Noves Bis-Tris 4-
102 12% gels using MES (2-(*N*-morpholino)ethanesulfonic acid) buffer at 200V for
103 40min and transferred to 0.4μm nitrocellulose membranes at 1.3A, 25V for 15min
104 using semidry transfer apparatus (BioRad). After protein transfer, membranes were
105 blocked in 5% non-fat dry milk in Tris-buffered saline with 1% Tween-20 (TBS-T)
106 for 30min. Primary antibodies were diluted in 5% BSA in TBS-T and western blots
107 were incubated in primary antibody for either 1hr at room temperature or
108 overnight at 4°C on a rocker. Western blots were then washed twice in TBS-T for
109 5min each time, followed by secondary antibody incubation using Li-Cor near
110 infrared fluorescence secondary antibodies. All blots were scanned using Li-Cor's
111 Near-InfraRed fluosrescence Odyssey CLx Imaging System with the exception of any
112 goat primary antibody which was visualized by chemiluminescence using BioRad's
113 Clarity Western ECL Substrate kit and Chemidoc XRS+ system. A complete list of all
114 primary and secondary antibodies used is listed in **Supp Table 5.** Protein

115 densitometry measurement was performed using Li-Cor's in-house ImageStudio
116 software.
117
118 *Immunofluoresecence*
119 Cells were plated on glass coverslips and were grown for 48hrs prior to any
120 starvation or drug treatment. After treatment, cells were fixed with 4% (w/v)
121 paraformaldehyde (Electron Microscopy Sciences) for 15min. Cells were
122 permeabilized using 0.1% Triton X-100 in PBS for all endogenous protein staining
123 except for LC3 staining. For endogenous LC3 staining, cells were first fixed in 4%
124 paraformaldehyde followed by 100% methanol for 10min. Cells were blocked in
125 1% BSA in PBS for 20min. Primary antibody staining was performed for 1hr in 1%
126 BSA in PBS, followed by two PBS washes for 5min each. Secondary antibody staining
127 was performed for 30min using Alexa Fluor Dyes (Molecular Probes) in 1% BSA in
128 PBS. Coverslips were mounted onto glass slide using ProLong Gold antifade reagent
129 with or without DAPI for nuclear staining. Images were taken using Zeiss LSM 710
130 Axio Observer confocal microscope with x63 objective lens. A complete list of all
131 primary and secondary antibodies used is listed in **Supp Table 5.**
132
133 *Flow Cytometry Analysis of EATR cells*
134 After treatment, cells were trypsinized and resuspended in complete media without
135 fixation for immediate flow cytometry analysis. All EATR ER-phagy experiments
136 were analysed with live cells because we found that cell permeabilization and
137 fixation reverses eGFP quenching due to loss of lysosomal acidification. On average,

138 5,000 mCherry and eGFP positive cells were analyzed per each sample. Data were
139 analysed using FlowJo software. Single cells were gated based on eGFP and mCherry
140 fluorescence intensity at fed condition to determine the 'Acidified ER' gate. Cells that
141 undergo ER-phagy is defined and quantified based on the shift of cell population
142 into the 'Acidified ER' gate due to loss of eGFP fluorescence.
143
144 *Immunoprecipitation*
145 Co-immunoprecipitation of LC3 with HA-FAM134B or HA-ATL2 was performed in
146 HEK293T cells by transient transfection with 10μg of plasmid for 24hrs. Co-
147 immunoprecipitation of ATL3 with HA-ATL2 constructs were performed in HCT116
148 cells stably expressing the different HA-ATL2 mutant constructs.
149 Immunoprecipitation of all HA-cDNA was performed using the Pierce Anti-HA
150 Magnetic Beads Kit (ThermoScientific) according to manufacturer's instruction.
151 Briefly, cells were lysed using the IP-lysis buffer supplemented with Halt Protease
152 Inhibitor Cocktail (ThermoFisher) and Halt Phosphatase inhibitor cocktail
153 (ThermoFisher). Equal amount of lysates (~5mg) were used to perform
154 immunoprecipitation using 50μl of HA-magnetic bead slurry. Immunoprecipitation
155 was performed at 4'C for 2hrs. The beads were washed twice using 'high-salt' IP
156 lysis buffer (IP lysis buffer supplemented with 500mM NaCl), with 5min incubation
157 on a rotor. The final wash was performed using regular IP lysis buffer.
158 Immunoprecipitated proteins were eluted by boiling the samples at 98'C in 1x
159 NuPAGE™ LDS Sample Buffer (thermoFisher) for 5min supplemented with NU-PAGE
160 sample reducing agent at final 1x concentration.

1. Horlbeck, M. A. *et al.* Compact and highly active next-generation libraries for CRISPR-mediated gene repression and activation. *eLife* **5,** 914 (2016).
2. Gibson, D. G. *et al.* Enzymatic assembly of DNA molecules up to several hundred kilobases. *Nat Meth* **6,** 343–345 (2009).

Figure 1: Development of sensitive and quantitative assays to measure ER-phagy

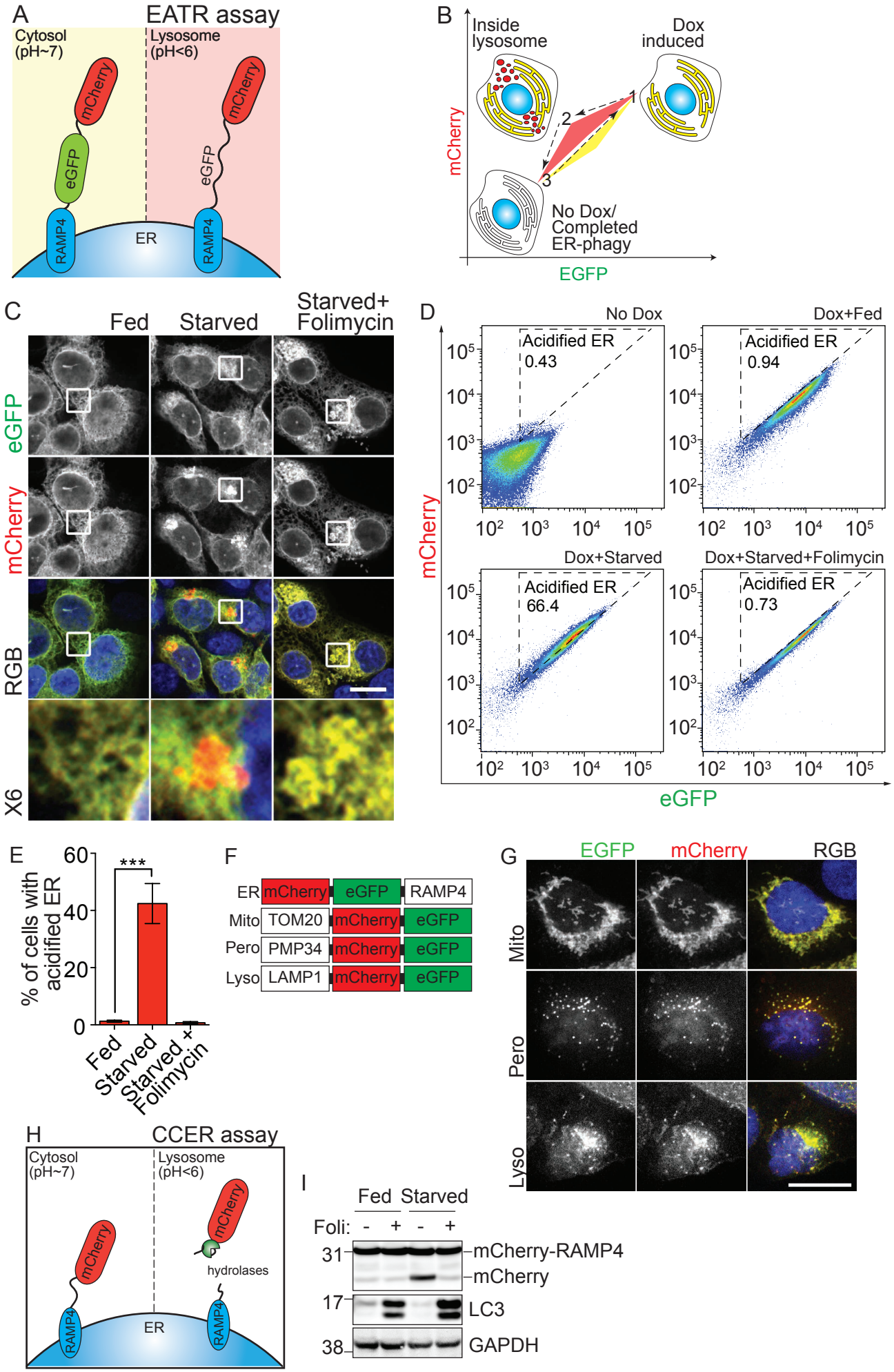

Figure 2: EATR and CCER detect changes in ER-phagy induced by manipulation of a known ER-phagy receptor Er-phagy

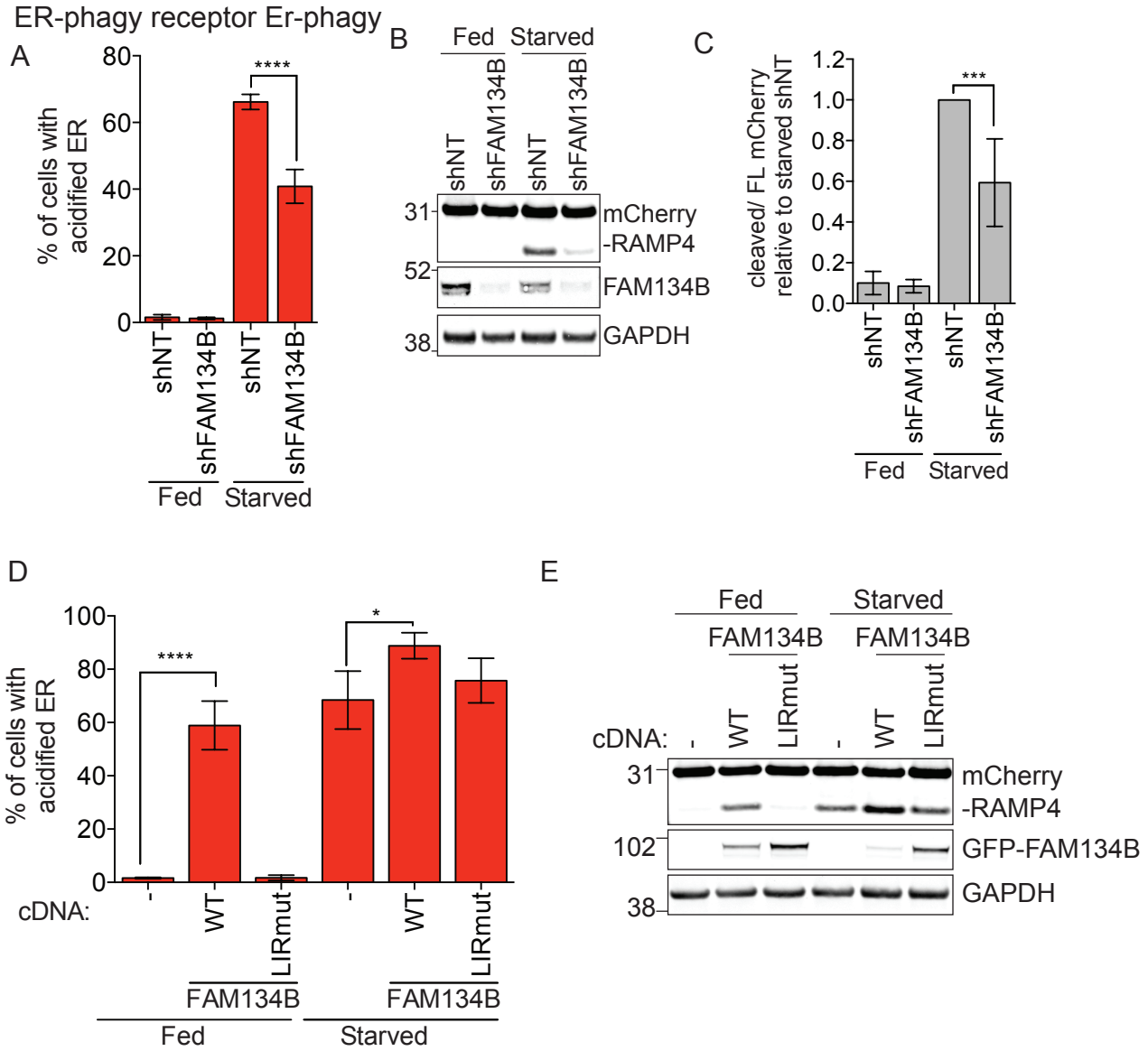

Figure 3: Atlastin knockdown inhibits ER-phagy

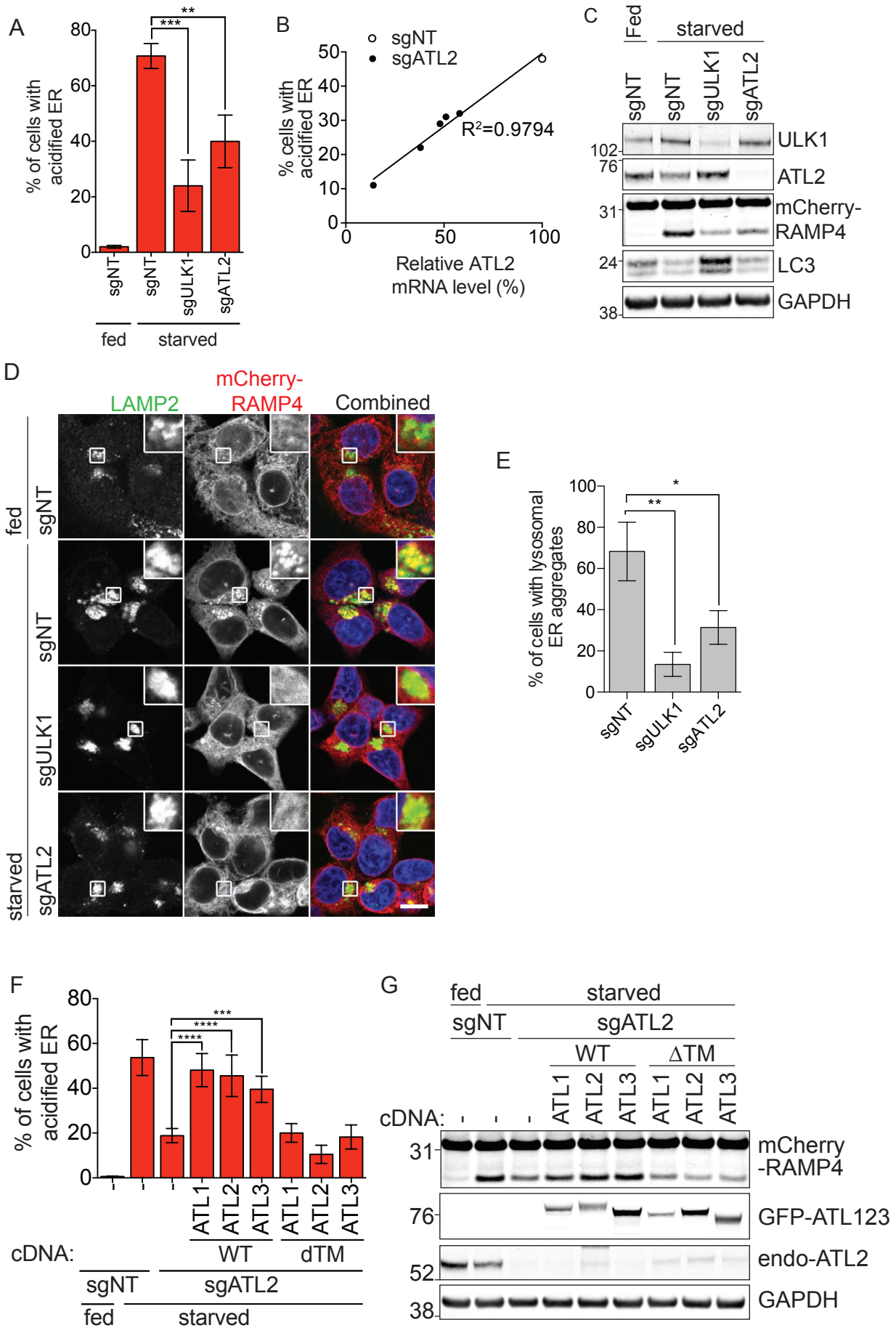

Figure 4: Atlastins act downstream of FAM134B-mediated ER-phagy

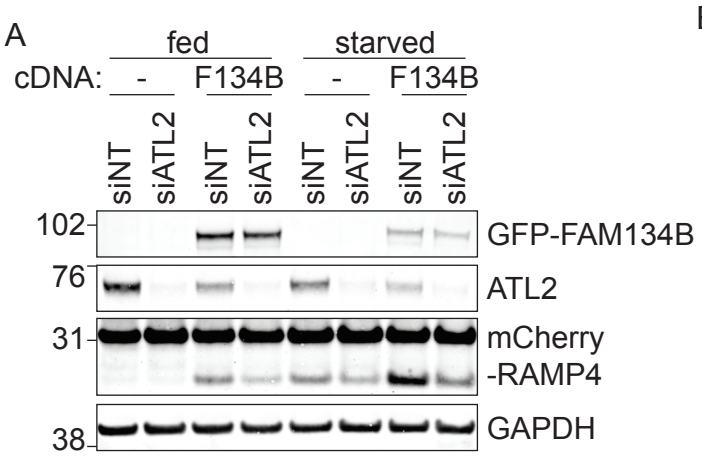

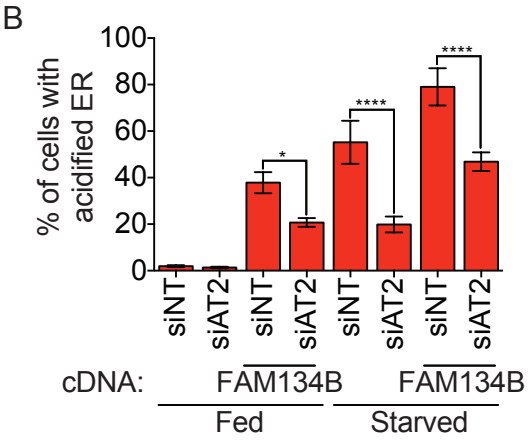
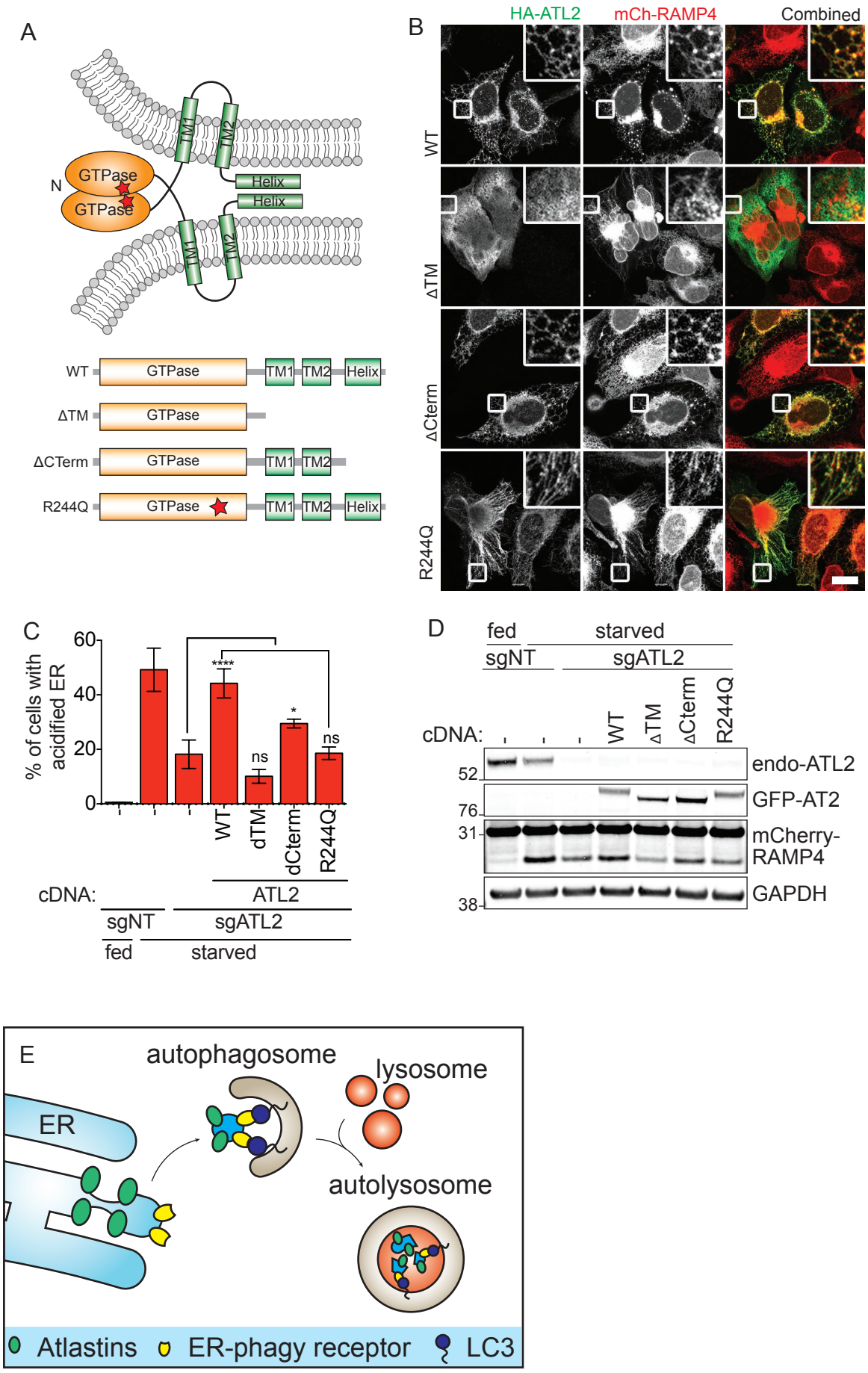
Figure 5: ER-phagy requires a functional Atlastin GTPase domain and proper ER localization